ISSN 1674-1056
http://cpb.iphy.ac.cn
http://iopscience.iop.org/cpb
中国物理 B
Chinese Physics
中国物理 Chinese Physics B

Size effect of Si particles on the electrochemical performances of Si/C composite anodes

Bonan Liu(刘柏男), Hao Lu(陆浩), Geng Chu(褚赓), Fei Luo(罗飞), Jieyun Zheng(郑杰允), Shimou Chen(陈仕谋), Hong Li(李泓)

Citation: Chin. Phys. B . 2018, 27(8): 088201. **doi:** 10.1088/1674-1056/27/8/088201

Journal homepage: http://cpb.iphy.ac.cn; http://iopscience.iop.org/cpb

What follows is a list of articles you may be interested in

A high-performance rechargeable Li-O_2 battery with quasi-solid-state electrolyte

Jia-Yue Peng(彭佳悦), Jie Huang(黄杰), Wen-Jun Li(李文俊), Yi Wang(王怡), Xiqian Yu(禹习谦), Yongsheng Hu(胡勇胜), Liquan Chen(陈立泉), Hong Li(李泓)

Chin. Phys. B . 2018, 27(7): 078201. **doi:** 10.1088/1674-1056/27/7/078201

Tuning hybrid liquid/solid electrolytes by lowering Li salt concentration for lithium batteries

Wei Yang(杨伟), Qi-Di Wang(王启迪), Yu Lei(雷宇), Zi-Pei Wan(万子裴), Lei Qin(秦磊), Wei Yu(余唯), Ru-Liang Liu(刘如亮), Deng-Yun Zhai(翟登云), Hong Li(李泓), Bao-Hua Li(李宝华), Fei-Yu Kang(康飞宇)

Chin. Phys. B . 2018, 27(6): 068201. **doi:** 10.1088/1674-1056/27/6/068201

Enhanced ionic conductivity in LAGP/LATP composite electrolyte

Shi-Gang Ling(凌仕刚), Jia-Yue Peng(彭佳悦), Qi Yang(杨琪), Ji-Liang Qiu(邱纪亮), Jia-Ze Lu(卢嘉泽), Hong Li(李泓)

Chin. Phys. B . 2018, 27(3): 038201. **doi:** 10.1088/1674-1056/27/3/038201

Gas treatment protection of metallic lithium anode

Wen-jun Li(李文俊), Quan Li(李泉), Jie Huang(黄杰), Jia-yue Peng(彭佳悦), Geng Chu(褚赓), Ya-xiang Lu(陆雅翔), Jie-yun Zheng(郑杰允), Hong Li(李泓)

Chin. Phys. B . 2017, 26(8): 088202. **doi:** 10.1088/1674-1056/26/8/088202

Conductivity and applications of Li-biphenyl-1, 2-dimethoxyethane solution for lithium ion batteries

Geng Chu(褚赓), Bo-Nan Liu(刘柏男), Fei Luo(罗飞), Wen-Jun Li(李文俊), Hao Lu(陆浩), Li-Quan Chen(陈立泉), Hong Li(李泓)

Chin. Phys. B . 2017, 26(7): 078201. **doi:** 10.1088/1674-1056/26/7/078201

Size effect of Si particles on the electrochemical performances of Si/C composite anodes*

Bonan Liu(刘柏男)[1,2], Hao Lu(陆浩)[1,2], Geng Chu(褚赓)[3], Fei Luo(罗飞)[4], Jieyun Zheng(郑杰允)[1], Shimou Chen(陈仕谋)[3], and Hong Li(李泓)[1,2,†]

[1] *Beijing National Laboratory for Condensed Matter Physics, Institute of Physics, Chinese Academy of Sciences, Beijing* 100190, *China*

[2] *School of Physical Sciences, University of Chinese Academy of Sciences, Beijing* 100049, *China*

[3] *Key Laboratory of Green Process Engineering, State Key Laboratory of Multiphase Complex Systems, Institute of Process Engineering, Chinese Academy of Sciences, Beijing* 100190, *China*

[4] *Tianmu Energy Anode Material Ltd. Co., Changzhou* 213300, *China*

(Received 29 April 2018; revised manuscript received 24 May 2018; published online 10 July 2018)

A series of Si/C composites were fabricated based on pitch and Si powders with particle sizes of 30, 100, 500, and 3000 nm. The size effects of the Si particles in the Si/C composites were investigated for lithium-ion battery anodes. The nanoscale Si and Si/C composites exhibited good capacity retentions. Scanning electron microscopy showed that exterior and interior cracks emerging owing to volume expansion as well as parasitic reactions with the electrolyte could well explain the performance failure.

Keywords: silicon–carbon composite, solid–electrolyte interphase, size effect, anode, volume expansion

PACS: 82.47.Aa, 65.40.gk, 82.45.Fk, 62.23.Pq **DOI:** 10.1088/1674-1056/27/8/088201

1. Introduction

Since their first commercialization in the 1990s, lithium-ion batteries (LIBs) have gradually occupied the portable-electronics market owing to their advantages of a high energy density, good rate capability, long cycle life, and low self-discharge rate. Nowadays, lithium-ion batteries are widely regarded as promising for various applications including electric vehicles, large-scale energy-storage equipment, distributed mobile power supply, and other fields.[1–3]

As an indispensable component in LIBs, the anode plays a significant role in determining the key parameters, such as cycle stability, energy density, and safety performance. Extensive efforts have been devoted to the investigation of anode materials in the past few decades, and significant progress has been achieved. Coke is the first commercialized LIB anode material, which provides a reversible capacity of 200 mAh/g–250 mAh/g. Afterwards, graphite became an important anode material owing to the large capacity of 372 mAh/g.[4] The successful commercialization of graphite can be attributed mainly to the significant improvements in electrolyte systems.[5] Graphite materials correspond to over 95% of the LIB market owing to the superior stability and high reversibility. After decades of development, the practical capacity of graphite can reach 340 mAh/g–370 mAh/g, approaching its theoretical energy-density limit. Therefore, the development of novel anode materials is necessary for future battery designs.

Silicon-based materials are the most-promising anode materials owing to the extremely high theoretical capacity of 3580 mAh/g for the formation of $Li_{15}Si_4$.[6,7] Si-based anodes exhibit an appropriate operation voltage of 0.4 V–0.5 V versus Li^+/Li, benign environmental properties, and low cost, which further increase their potentials. However, two main challenges have hindered wide applications of Si-based anodes. One of them is the volume inflation;[8,9] the volume expansion of silicon during lithiation and de-lithiation can reach up to 320%,[10] which is linearly proportional to the lithiation amount, irrespective of the particle size, morphology, or crystallinity.[11,12] The large stress and strain induced from volume changes would lead to cracking of active particles, exposure of fresh surfaces, and exfoliation of the electrode. The other challenge is the formation of an inhomogeneous and unstable solid–electrolyte–interphase (SEI) layer on silicon anodes during electrochemical cycling.[13] The SEI would continuously grow whenever a fresh surface is exposed owing to volume swell. The SEI on a silicon anode could grow to a thickness of several micrometers after dozens of cycles.[14] The unstable SEI hindered practical applications. In full cells, the continuous growth of unstable SEI rapidly consumes the limited lithium and electrolyte, leading to a fast capacity decay.[15,16]

In order to overcome these issues, several approaches have been proposed. The nano-silicon/carbon composite material, composed of well-dispersed nanoscale silicon in a carbon matrix, is one of the most-promising candidates.[17,18]

*Project supported from the "Strategic Priority Research Program" of the Chinese Academy of Sciences (Grant No. XDA09010102).

†Corresponding author. E-mail: hli@iphy.ac.cn

© 2018 Chinese Physical Society and IOP Publishing Ltd

The cracking mechanism and size effect of Si have been thoroughly studied in pure-Si systems. Surface cracking emerges during lithiation of silicon, which can be attributed to the large hoop tension in the outer layers of the particles.[19–23] Early studies confirmed that the critical size, below which the cracking did not occur, was ∼150 nm for crystalline Si and ∼870 nm for amorphous Si based on a transmission electron microscopy (TEM) characterization and mechanical simulations.[24,25] However, no extensive studies of the size effect of Si on the formation of cracks in Si/C composite materials have been reported. In this study, we synthesized a series of Si/C composites based on pitch and Si powders with sizes of 30, 100, 500, and 3000 nm. The electrochemical performances of these Si/C composite materials are studied. Scanning electron microscopy (SEM) measurements are employed to investigate the external and internal structures, and crack evolutions during different cycles.

2. Experimental methods

2.1. Synthesis

Si particles with sizes of 30 nm and 100 nm (Alfa Aesar) were laser-synthesized from vapor phase. Si particles with larger sizes of 500 nm and 3 μm were obtained through jet milling from 325-mesh-silicon powder (Alfa Aesar).

The precursors for the Si/C composites are silicon powders with different sizes of 30, 100, 500, and 3000 nm, and coal pitch. The pitch has a softening point of 200 °C and coking value larger than 70%. A mixture of Si and pitch with a weight ratio of 1:9 was sintered in a rotary kiln at 900 °C for 2 h to ensure uniform coating and carbonization of the pitch.

2.2. Electrochemical measurements

The pure-Si electrode contained 70 wt% of silicon, 20 wt% of CB, and 10 wt% of CMC. The Si/C composite electrodes were prepared with 93 wt% of Si/C active material, 2 wt% of carbon nanotubes as conductive additives, 2 wt% of Na–CMC, and 3 wt% of styrene-butadiene rubber (SBR) as binders. A slurry of the above mixture with deionized water was cast on a Cu foil current collector and then dried at 100 °C. Electrodes with dimensions of 8 mm×8 mm were punched and dried under a vacuum at 110 °C overnight to remove traces of water and then introduced in an argon-filled glove-box. The weights of active material per electrode were approximately 0.3 mg/cm^2 and 3 mg/cm^2 for pure Si and Si/C, respectively. The electrolyte was a solution of 1-M $LiPF_6$ in ethylene carbonate (EC) and dimethyl carbonate (DMC) (1:1 in volume) with 5% fluoroethylene carbonate (FEC) as an additive. The addition of FEC could help stabilize the SEI. A lithium foil was used as the counter electrode, while glass fiber was used as the separator. 2032-type coin cells were assembled in an argon-filled glove box.

Discharge and charge tests were performed on a Land BT2001 battery test system (Wuhan, China) in a voltage range of 0.005 V–1 V at various C-rates at room temperature (1 C corresponds to a current density of 0.6 A/g). Electrochemical impedance spectroscopy (EIS) measurements were performed at 1.0 V using an electrochemical workstation (CHI660B) with an amplitude of the AC signal of 5 mV in a frequency range of 4 MHz to 0.1 Hz.

2.3. Characterizations

The phase compositions of Si and Si/C were characterized using an x-ray diffractometer (D8 Advance, Bruker) equipped with a Cu–K_α radiation source in a scan range (2θ) of 10°–80° with an increment of 0.02°.

The size distributions of the 30-nm and 100-nm silicon particles were evaluated by TEM (FEI20). The samples were dispersed in alcohol and deposited on a carbon film.

After different numbers of cycles (1st, 10th, 20th, 50th, and 100th cycle) at the cut-off voltage of 1.0 V, the coin cells were disassembled in the glove box with a disassemble machine (MSK-110, MTI, China). The electrodes were washed at least three times with DMC and then dried in a vacuum box for at least 4 h. The morphologies of the surface and focused ion beam (FIB) prepared cross-section were investigated with an SEM (Hitachi S-4800) equipped with an energy-dispersive x-ray spectroscopy (EDS) setup. In order to avoid air contamination, all of the measurements and transfer processes were performed under an Ar atmosphere or vacuum environment.

3. Results and discussion

3.1. Morphology and electrochemical properties of the pure Si anode

Figure 1 shows the morphologies of the Si particles with different sizes. The Si particles with average sizes of 30 nm (Figs. 1(a) and 1(c)) and 100 nm (Figs. 1(b) and 1(d)) have narrow particle-size distributions and spherical shapes. The Si particles with larger sizes of 500 nm (Fig. 1(e)) and 3 μm (Fig. 1(f)) exhibit irregular shapes. The x-ray diffraction (XRD) patterns in Fig. 2 verify the phase purity of the four samples. The peak of the 30-nm Si is wider owing to the smaller grain and particle sizes.

The charging and discharging curves and electrochemical performances of the pure-Si samples with different particle sizes are shown in Fig. 3. The charging capacity attributed to the SEI was larger for Si with the sizes of 30 nm and 100 nm, owing to the larger surface area. In addition, it is worth noting that the de-lithiation platform in the discharging curve is oblique for the smaller Si particles owing to the size effect on the surface energy.[26] Their initial discharge capacities are approximately equal, with values of approximately 3200 mAh/g–3300 mAh/g. After 100 cycles, the discharge

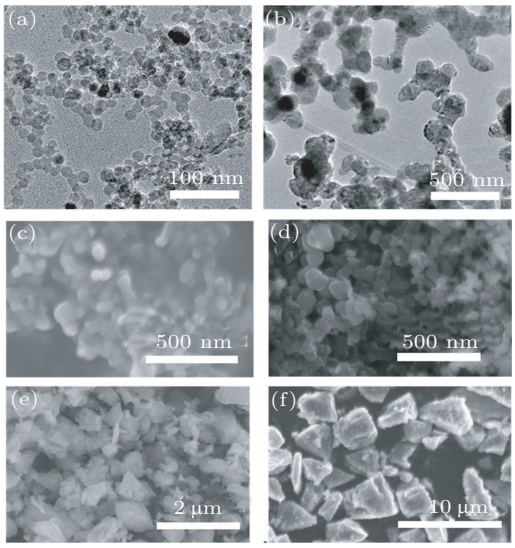


Fig. 1. (color online) TEM images of Si particles with sizes of (a) 30 nm and (b) 100 nm. SEM images of Si particles with sizes of (a) 30 nm, (b) 100 nm, (c) 500 nm, and (d) 3 μm.

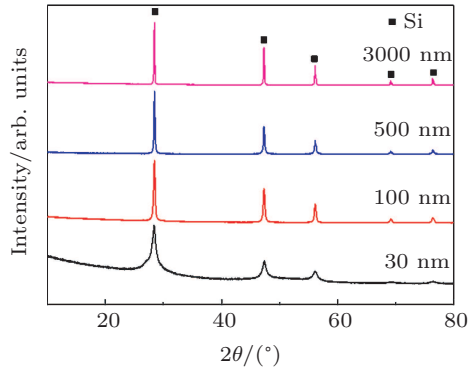


Fig. 2. (color online) XRD patterns of the Si particles with average sizes of 30 nm, 100 nm, 500 nm, and 3 μm.

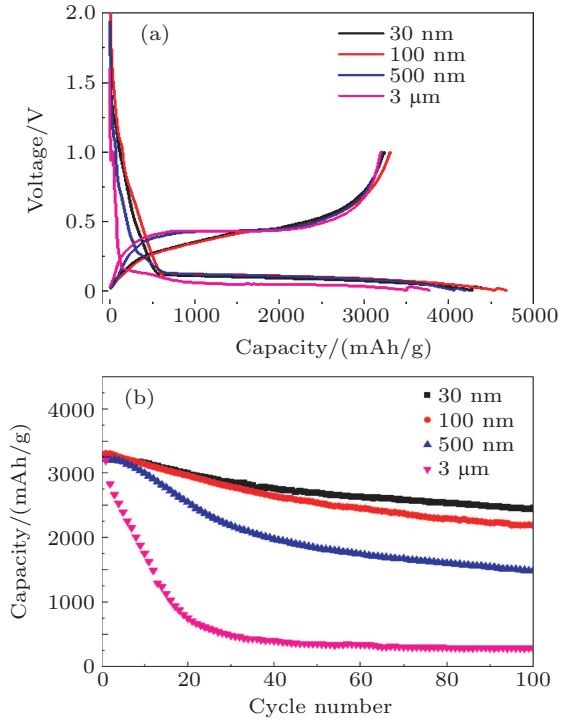


Fig. 3. (color online) (a) Charging and discharging curves of the first cycle and (b) cycling performances of the Si particles with different sizes at a current density of 0.2 A/g in the voltage window of 0.005 V–1 V.

capacities of the Si samples with the particle sizes of 30 nm, 100 nm, 500 nm, and 3 μm decrease to 2454, 2189, 1483, and 279 mAh/g, respectively. The Si particles with smaller sizes exhibit significantly better capacity-retention behaviors. This result is consistent with a previous report by Li *et al.*[27] They reported that the volume variation of single nanometer alloy particles was significantly smaller than that of single large-size alloy particles during discharge–charge cycles. Moreover, the higher plasticity and deformability of nanomaterials prevent electrode cracking and pulverization.

3.2. Morphology and electrochemical properties of the Si/C composites

The XRD patterns of the Si/C composites are typical patterns of a simple physical mixture of components: silicon and pitch coke (Fig. 4); no silicon–carbide formation was detected upon heat-treatment.

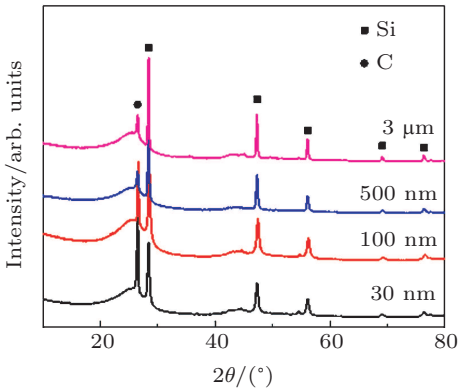


Fig. 4. (color online) XRD patterns of the Si/C composites with Si particle sizes of 30 nm, 100 nm, 500 nm, and 3 μm.

Figure 5 reveals the morphologies of the Si/C composites containing Si particles with different sizes. It is worth noting that after the calcination process with pitch melting, the Si/C composites have microscale sizes in the range of 10 μm–15 μm with "potato-like" shapes; they have a wide size distribution. The pristine Si particles are difficult to be identified, which implies that the pitch-derived carbon successfully wraps them; the Si particles are well dispersed in the carbon matrix.

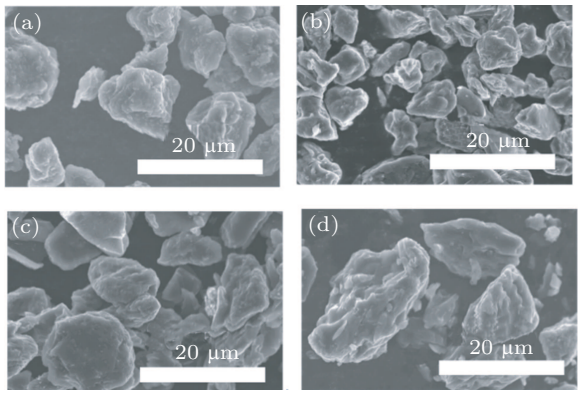


Fig. 5. (color online) SEM images of the Si/C composites with Si particle sizes of (a) 30 nm, (b) 100 nm, (c) 500 nm, and (d) 3 μm.

The electrochemical performances of the Si/C composites were evaluated; the results are shown in Fig. 6. It should be mentioned that the areal capacity of the electrode is 2.5 mAh/cm^2, close to the practical application level. The charging and discharging curves demonstrate a combination of Si and soft carbon, particularly in the discharging curve.[28] In the dQ/dV curves (Fig. 6(b)), the peaks at ~0.42 V are higher for the 500-nm and 3-μm Si/C, consistent with the conclusion from Fig. 3(a), indicating that the size and structure of silicon have not been altered during the sintering and milling of Si/C. The capacity variations of these Si/C composites as a function of the cycling time are shown in Fig. 6(c). All of the Si/C composites deliver initial discharge capacities of approximately 600 mAh/g, corresponding to 12 wt% of silicon, considering that the theoretical capacity of Si is 3200 mAh/g and that the theoretical capacity of the pitch-derived carbon is 250 mAh/g. The cycling performance deteriorates with the increase of the Si particle size. The initial discharge capacities are 605, 586, 592, and 584 mAh/g for the 30-nm, 100-nm, 500-nm, and 3-μm Si/C, with corresponding capacity retentions of 87.5%, 81.4%, 67.2%, and 48.1%, respectively, after 100 cycles. In line with the pure Si anode, the Si particles with smaller sizes in the composites deliver better electrochemical performances. A better capacity-retention capability is accompanied with a high Coulombic efficiency, as demonstrated in Fig. 6(d). The average Coulombic efficiencies of the 10th–100th cycles for the 30-nm, 100-nm, 500-nm, and 3-μm Si/C are 99.3%, 98.9%, 98.6%, and 98%, respectively. In summary, the Si/C composite with a smaller Si particle size has a better capacity retention upon the discharge–charge processes.

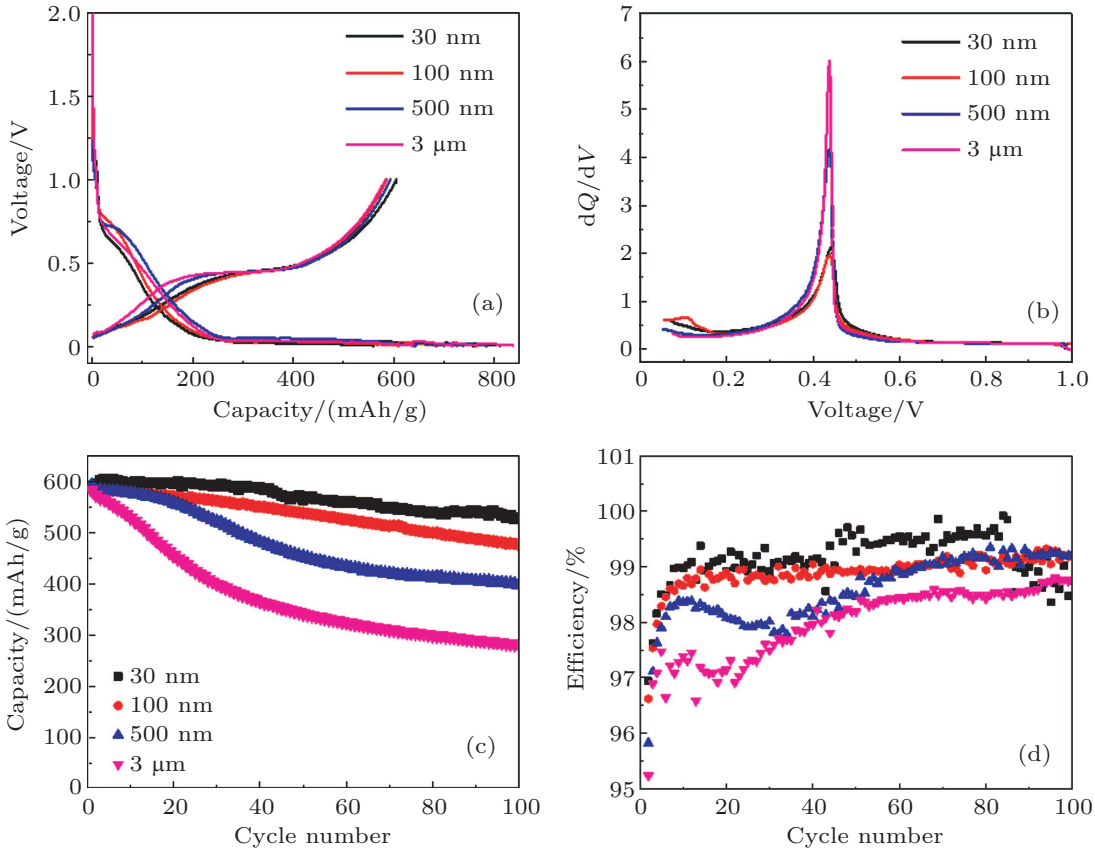


Fig. 6. (color online) (a) Charging and discharging curves of the first cycle and (b) dQ/dV curves corresponding to the de-lithiation process. (c) Cycling performances and (d) Coulombic efficiencies of the Si/C composites as a function of the number of cycles at a current density of 0.12 A/g in the voltage window of 0.005 V–1 V.

3.3. Morphology evolutions of the Si/C composites

It is known that Si suffers from a large volume expansion during lithium insertion, which may lose contact with the conductive materials and lead to a high polarization. The exposed fresh surface-active materials can promote side reactions with the electrolytes, consuming the electrolyte and causing a low Coulombic efficiency. In this study, we track the surface morphology evolutions of the electrodes after different numbers of cycles (1st, 20th, 50th, and 100th cycle), as shown in Fig. 7. The 30-nm and 100-nm Si/C composites remain flawless after the first cycle. With the increase of the number of cycles, the number of cracks generated in the electrodes increases. For the 500-nm and 3-μm Si/C composites, cracks can be observed in the electrodes just after the first cycle. After 20 cycles, the particles are completely torn by the large volume expansion/contraction during the cycling. It is worth noting that the electrodes of the 500-nm and 3-μm Si/C composites were pulverized when we disassembled the cells.

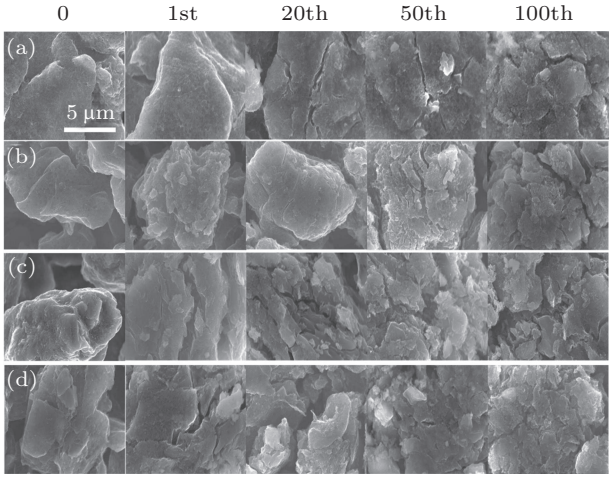


Fig. 7. (color online) Surface morphology evolutions of the Si/C composites after different numbers of cycles at the cut-off voltage of 1.0 V: (a) 30-nm, (b) 100-nm, (c) 500-nm, and (d) 3-μm Si/C. The scale bar corresponds to 5 μm.

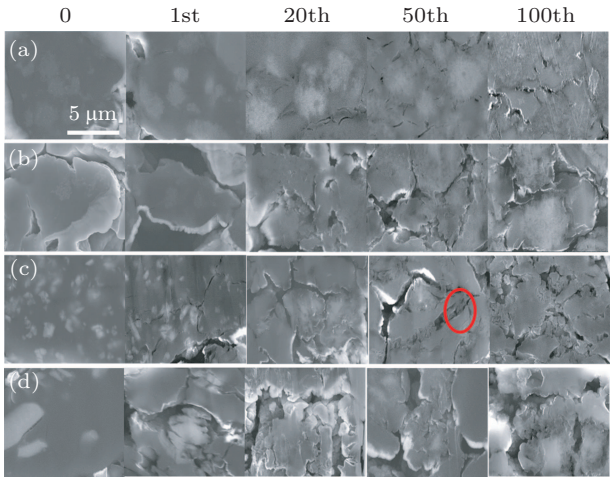


Fig. 8. (color online) Internal morphology evolutions of the Si/C composites after different numbers of cycles at the cut-off voltage of 1.0 V: (a) 30-nm, (b) 100-nm, (c) 500-nm, and (d) 3-μm Si/C. The scale bar corresponds to 5 μm.

The Si particles are wrapped by the pitch-derived carbon; it is necessary to understand the internal cracking within particles. Using FIB techniques, we obtained the cross-sections of the Si/C composites (Fig. 8). For the 30-nm Si/C composite (Fig. 8(a)), the silicon particles slightly aggregate inside the carbon matrix owing to their high specific surface area. This composite can be divided into an Si-rich part and C-rich part. Based on the SEM image, there are no obvious cracks after the 1st cycle. After 20 cycles, it has cracks, consistent with the surface morphology. It is worth mentioning that the cracks emerge in the C-rich part rather than in the Si-rich part. Even after prolonged cycles, large cracks were not observed in the Si-rich part. The Si-rich part was blurred after 100 cycles, owing to a large amount of SEI, as discussed below. The 100-nm Si/C composite has a similar behavior to that of the 30-nm Si/C composite (Fig. 8(b)); however, a larger cleavage and smaller fractured-particle size are observed. The cracks did not propagate along the Si/C interface. For the 500-nm Si/C composite, no Si aggregation is observed owing to the large size of the silicon particles. Cracks appear after the first cycle, but do not exacerbate at the Si/C interface; no obvious cracks in silicon were observed until the 20th cycle. The width of the cracks could exceed 500 nm after 50 cycles (red circle). Inside the cleavage, SEI grows inside the crack after prolonged cycles. The surrounding carbon matrix may decrease the hoop tension, as reported by Huang *et al.* who revealed that the carbon matrix can alleviate the volume expansion of SnO.[29] The 500-nm Si/C composite is rapidly torn; silicon particles were fractured and detached from the matrix (Fig. 8(d)). This well explains its lower capacity retention and lower Coulombic efficiency, as demonstrated in Fig. 6. Larger silicon particles yield a larger stress on the carbon matrix leading to a faster fracture. It is worth noting that even when the silicon size is as small as 30 nm, the composite still fails under the large stress.

3.4. SEI formation and impedance

Energy-dispersive spectrometry (EDS) is employed to analyze the C, Si, and F elemental distributions for the 30-nm Si/C composite after 20 and 100 cycles (Fig. 9). It reveals that the points A and C are C-rich areas, while the points B and D are Si-rich areas. After 20 cycles, there is a small F-element signal at the point A, suggesting almost no formation of SEI. As the electrolyte contains 5% of FEC and the electrode was rinsed thoroughly with DMC, the F element should mainly originate from the SEI. After 100 cycles, the whole F content increases from 1.3% to 9.95%, indicating the formation of a large amount of SEI. In addition, for the Si-rich part inside the particle, the content of F significantly increases to 11.08%. As shown in Fig. 8, the Si-rich part blurred after 100 cycles. Once the composite material cracks, the electrolyte would permeate inside the particles leading to a continuous growth of SEI. The EDS results are shown in Table 1.

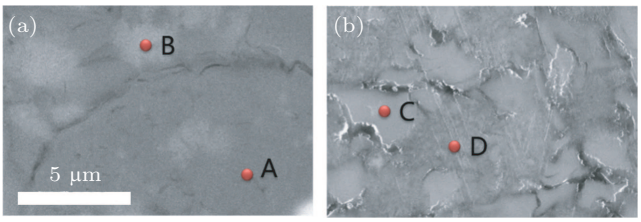


Fig. 9. (color online) Cross-section SEM images of the 30-nm Si/C composite after (a) 20 cycles and (b) 100 cycles. The scale bar corresponds to 5 μm.

Table 1. EDS results based on the area of Fig. 7.

	C	Si	F
Area (a)	85.16	5.39	1.03
Point A	96.74	0.56	–
Point B	65.46	22.39	0.66
Area (b)	70.58	7.41	9.95
Point C	86.91	2.65	4.99
Point D	60.23	12.13	11.08

The EIS with Nyquist plots of the Si/C composites after different numbers of cycles at the cut-off voltage of 1.0 V, and corresponding R_{ct} and R_{SEI} evolutions obtained using an equivalent-circuit fitting are presented in Fig. 10. Overall, after the activation process with a decreasing R_{ct} in the first 20 cycles, the R_{ct} gradually increases; the 3-μm Si/C composite has the largest R_{ct} of 390 Ω; that of the 30-nm Si/C composite is 150 Ω at the 100th cycle. This suggests that a worse electrical connection occurs, particularly at the large particle size owing to the crack formation. For the SEI, the R_{SEI} increases with the number of cycles, indicating a continuous formation of SEI in these composites. The 30-nm Si/C composite has the smallest R_{SEI}, which can well explain its high capacity and good cycling-duration performance.

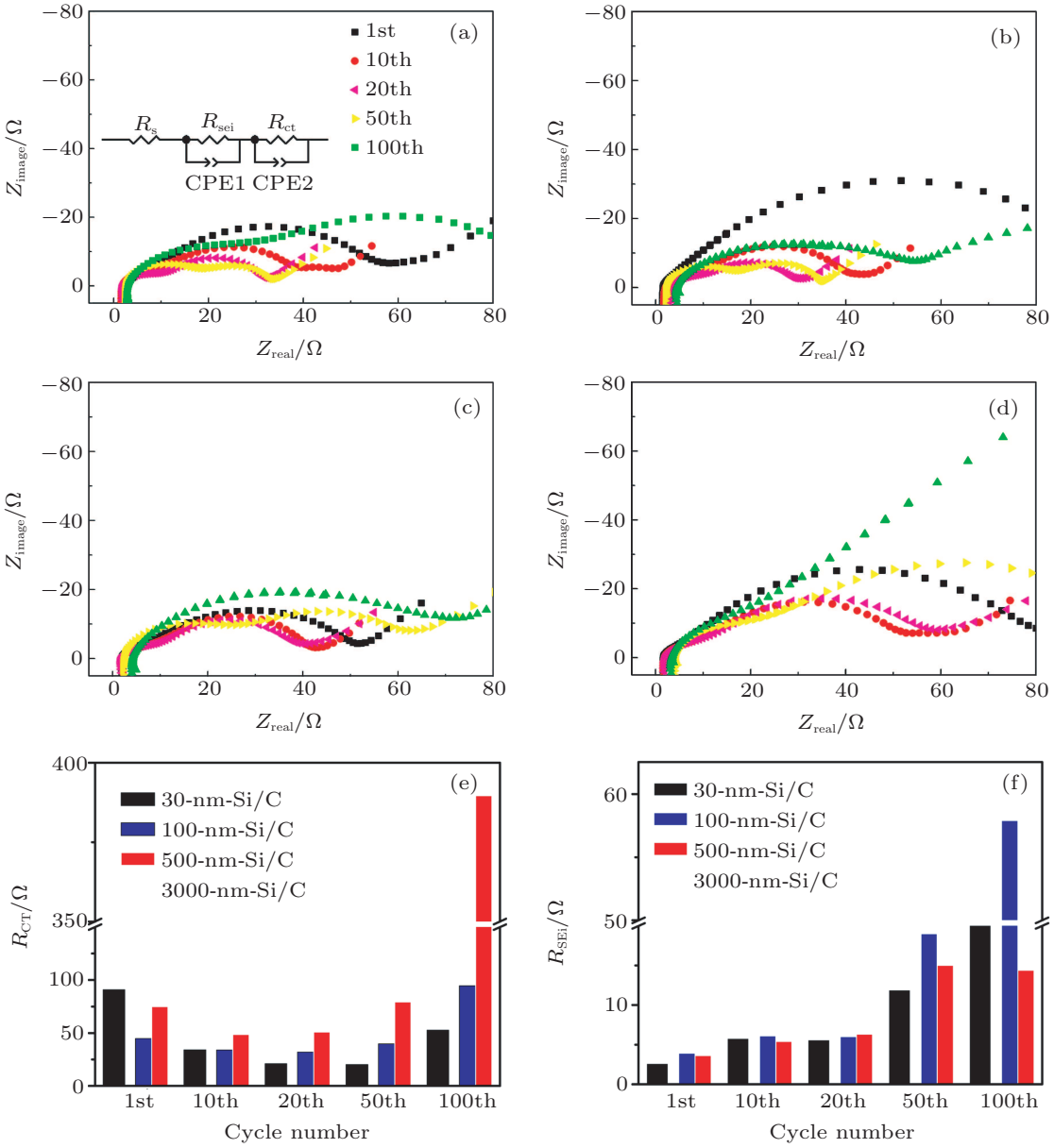


Fig. 10. (color online) EIS of the Si/C composites after different numbers of cycles at the cut-off voltage of 1.0 V: (a) 30-nm, (b) 100-nm, (c) 500-nm, and (d) 3000-nm Si/C. (e) Charge-transfer resistance evolutions as a function of the number of cycles for the composites. (f) SEI resistance evolution as a function of the number of cycles for the composites.

4. Conclusions

Si/C composites were fabricated by sintering petroleum pitch and Si with particle sizes of 30, 100, 500, and 3000 nm. Both pure Si and Si/C composites with the smallest particle size (30 nm) had the best capacity retentions as well as the smallest R_{SEI} increments. *Ex-situ* SEM assisted with the FIB technique demonstrated that the pitch-derived carbon could relieve the strain and stress of Si during cycling. Cracks were easily generated in the large particles during cycling; the cracks did not propagate along the Si/C interface, owing to the interplay between the interface strength and hoop tension. Once the composite cracks, electrolyte would permeate inside active particles and lead to a continuous growth of SEI, which is detrimental for the electrochemical performances of the Si/C

composite materials.

References

[1] Bridel J S, Azaïs T, Morcrette M, Tarascon J M and Larcher D 2010 *Chem. Mater.* **22** 1229

[2] Kierzek K, Machnikowski J and Béguin F 2014 *J. Appl. Electrochem.* **45** 1

[3] Luo F, Liu B, Zheng J Y, Chu G, Zhong K F, Li H, Huang X J and Chen L Q 2015 *J. Electrochem. Soc.* **162** A2509

[4] Flandrois S and Simon B 1999 *Carbon* **37** 165

[5] Xu K 2004 *Chem. Rev.* **104** 4303

[6] Hatchard T D and Dahn J R 2004 *J. Electrochem. Soc.* **151** A838

[7] Li J and Dahn J R 2007 *J. Electrochem. Soc.* **154** A156

[8] Pereira-Nabais C, Światowska J, Chagnes A, Ozanam F, Gohier A, Tran-Van P, Cojocaru C S, Cassir M and Marcus P 2013 *Appl. Surf. Sci.* **266** 5

[9] Philippe B, Dedryv'ere R, Allouche J, Lindgren F, Gorgoi M, Rensmo H, Gonbeau D and Edström K 2012 *Chem. Mater.* **24** 1107

[10] He Y, Yu X Q, Li G, Wang R, Li H, Wang Y L, Gao H J and Huang X J 2012 *J. Power Sources* **16** 131

[11] McDowell M T, Lee S W, Nix W D and Cui Y 2013 *Adv. Mater.* **25** 4966

[12] Obrovac M N and Chevrier V L 2014 *Chem. Rev.* **114** 11444

[13] Zheng J Y, Zheng H, Wang R, Ben L B, Lu W, Chen L W, Chen L Q and Li H 2014 *Phys. Chem. Chem. Phys.* **16** 13229

[14] Luo F, Chu G, Xia X X, Liu B N, Zheng J Y, Li J J, Li H, Gu C Z and Chen L Q 2015 *Nanoscale* **7** 7651

[15] Dupre N, Moreau P, De Vito E, Quazuguel L, Boniface M, Bordes A, Rudisch C, Bayle-Guillemaud P and Guyomard D 2016 *Chem. Mater.* **28** 2557

[16] Nguyen D T, Kang J, Nam K M, Paik Y and Song S W 2016 *J. Power Sources* **303** 150

[17] Holzapfel M, Buqa H, Krumeich F, Novák P, Petrat F M and Veit C 2005 *Electrochem. Solid State Lett.* **8** A516

[18] Terranova M L, Orlanducci S, Tamburri E, Guglielmotti V and Rossi M 2014 *J. Power Sources* **246** 167

[19] Zhao K, Pharr M, Wan Q, Wang W L, Kaxiras E, Vlassak J J and Suo Z G 2012 *J. Electrochem. Soc.* **159** A238

[20] Ma Z, Li T, Huang Y L, Liu J, Zhou Y and Xue D 2013 *RSC Adv.* **3** 7398

[21] Zhao K, Pharr M, Cai S, Vlassak J J and Suo Z G 2011 *J. Am. Ceram. Soc.* **94** 226

[22] Huang S, Fan F, Li J, Zhang S and Zhu T 2013 *Acta Mater.* **61** 4354

[23] Kalnaus S, Rhodes K and Daniel C 2011 *J. Power Sources* **196** 8116

[24] Liu X H, Zhong L, Huang S, Mao S X, Zhu T and Huang J Y 2012 *ACS Nano* **6** 1522

[25] McDowell M T, Lee S W, Harris J T, Korgel B A, Wang C, Nix W D and Cui Y 2013 *Nano Lett.* **13** 758

[26] Li H, Wang Z X, Huang X J and Chen L Q 2008 *Physics* **37** 416 (in Chinese)

[27] Li H, Huang X J, Chen L Q, Wu Z G and Liang Y 1999 *Electrochem. Solid State Lett.* **2** 547

[28] Lu H, Liu B N, Chu G, Zheng J Y, Luo F, Qiu X P, Li H, Liu F, Feng S N, Chen W, Li H and Chen L Q 2016 *Energy Storage Science and Technology* **5** 109

[29] Zhang L Q, Liu X H, Liu Y, Huang S, Zhu T, Gui L, Mao S X, Ye Z Z, Wang C M, Sullivan J P and Huang J Y 2011 *ACS Nano* **5** 4800